Early Attempts at Physics Informed Machine learning (PIML) for Thermal Modelling of Wire arc additive manufacturing

Jagadeeswaran Murapaka

A Dissertation Submitted to

Indian Institute of Technology Hyderabad

In Partial Fulfillment of the Requirements for

The Degree of Master of Technology

भारतीय प्रौद्योगिकी संस्थान हैदराबाद

Indian Institute of Technology Hyderabad

Department of Interdisciplinary (Additive Manufacturing)

December, 2023

Declaration

I declare that this written submission represents my ideas in my own words, and where others' ideas or words have been included, I have adequately cited and referenced the original sources. I also declare that I have adhered to all principles of academic honesty and integrity and have not misrepresented or fabricated or falsified any idea/data/fact/source in my submission. I understand that any violation of the above will be a cause for disciplinary action by the Institute and can also evoke penal action from the sources that have thus not been properly cited, or from whom proper permission has not been taken when needed.

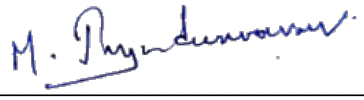

(Signature)

Jagadeeswaran Murapaka

AM22MTECH14001

Approval Sheet

This thesis entitled **Machine Learning approach for temperature mapping in Wire arc additive manufacturing** by JAGADEESWARAN MURAPAKA is approved for the degree of Master of Technology from IIT Hyderabad.

_____

Dr. Anurup Datta
Department of Mechanical and Aerospace Engineering
Indian Institute of Technology, Hyderabad
Examiner

_____

Prof. Amirtham Rajagopal
Department of Civil Engineering
Indian Institute of Technology, Hyderabad
Examiner

_____

Prof. Suryakumar S.
Department of Mechanical and Aerospace Engineering
Indian Institute of Technology, Hyderabad
Adviser

_____

Dr. J. Saketha Nath
Department of Computer Science and Engineering
Indian Institute of Technology, Hyderabad
Co-Adviser

Acknowledgements

I would like to express my special thanks of gratitude to my supervisor **Prof. Suryakumar S.,** Indian Institute of Technology, Hyderabad for giving me the golden opportunity to do this project and provide me the constant guidance throughout this work. I would also like to express my deep sense of thanks to my adviser **Dr. Saketha Nath Jagarlapudi** for providing me the directions in my project. It was a great privilege and honor to work under their guidance.

I would like to thank my fellow lab mates: Nagallpatti Vishwanath, Vishnu S, Ashutosh Yadav, Pranav, Siddharth, Aravind Krishnan for the discussions during weekly meetings.

Abstract

Machine learning, a rapidly advancing field, plays a significant role in additive manufacturing, a technology still in its development stages. Within the realm of large-scale additive manufacturing, Wire Arc Additive Manufacturing (WAAM) stands out due to its high deposition rate, wide material selection, and substantial productivity. However, WAAM faces challenges with residual stresses caused by large thermal gradients, which can distort the final product. To address this issue, Thermal modelling forms a basis to understand the thermal behavior of the part and helps in study of heat distribution and accumulation during the process which in turns are the major causes of residual stresses and distortion. This works aims to explore Physics informed machine learning model (PIML), specifically physics informed Neural Networks (PINNS) for the thermal modelling without or with very limited simulated data by incorporating the process physics.

Physics-Informed Neural Networks integrate the governing differential equations of heat transfer and their boundary conditions. This integration merges the reliability of physics-based models with the adaptability of neural networks, enabling real-time prediction of temperature distribution. This thesis delves into the expectations and potential of machine learning in enhancing additive manufacturing, particularly focusing on its future impact and significance.

Abbreviations

• WAAM Wire Arc Additive Manufacturing

• AM Additive Manufacturing

• ML Machine learning

• DED Direct Energy Deposition

• CNC Computer Numerical Control

• CMT Cold Metal Transfer

• PINN Physics Informed Neural Networks

- L-DED – Laser Directed energy deposition

Contents

List of Figures

List of Tables

Chapter 1

Introduction

1.1 Directed Energy Deposition

DED, or Directed Energy Deposition, is a method in additive manufacturing (AM) that involves initially using material in the form of wire or powder. A heat source, such as a laser, electric arc, or electron beam, is then employed to melt the material, allowing it to be deposited in a layer-by-layer manner. Among the various DED techniques, the most currently sought-after are WAAM (Wire Arc Additive Manufacturing) and Laser DED. WAAM, a specific type of DED, utilizes an arc as the heat source and wire as the feedstock. The movement of the welding torch is controlled by either a CNC setup or a robot. In this process, the wire is continuously supplied through a wire feed system. WAAM is particularly adept at creating components that are close to their final net shape.

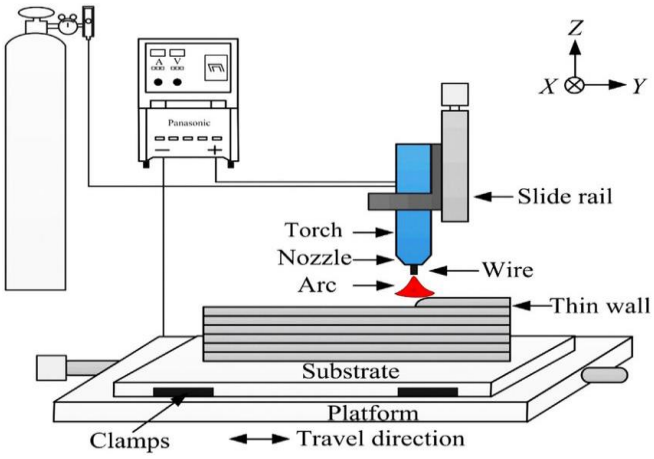

Fig 1.1. Schematic of Wire arc AM Process [1]

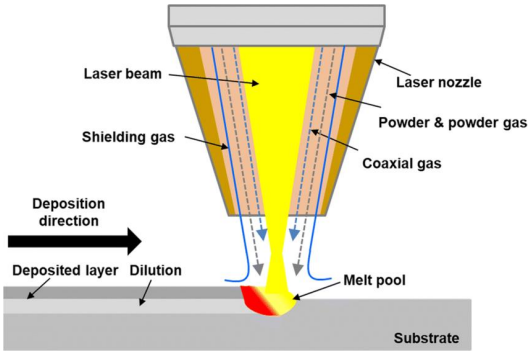

Fig1.2. Schematic of Laser Powder DED [2]

While WAAM offers numerous benefits, it commonly faces challenges such as residual stress and distortion. These issues arise due to the significant temperature differences, thermal strain, and residual stress that occur when a new layer is deposited on a cooler substrate or on a previously deposited layer. Such residual stresses can adversely affect the fatigue life and fracture toughness of the component, leading to problems like distortion, reduced geometric accuracy, and layer separation during the deposition process.

There are several techniques to mitigate residual stress in WAAM. These include preheating the substrate, using shorter deposition paths or depositing in smaller segments, employing effective deposition patterns such as inward spiraling, increasing the scanning speed, and reducing the height of each deposited layer. Notably, preheating the substrate can significantly reduce the stress developed during fabrication and the final residual stress. High preheating temperatures help in diminishing the strain by reducing the temperature differential and, consequently, the thermal strain. Moreover, this approach can also be beneficial in lowering the likelihood of solidification cracking. Adjusting the power and scanning speed are other viable methods to curtail residual stresses in the process.

1.2 Necessity of Physics based Machine Learning

- After thorough investigation from the literature, it has been found that traditional computational simulations are very expensive and time consuming. On the other hand, Data driven machine learning techniques are faster and

efficient but they are data hungry and required lot of simulated data from computational simulations. Therefore, data driven ML techniques are hugely dependent on computationally expensive simulated data. So here where physics informed neural networks (PINNS) can play vital role by incorporating the physics behind the process without using much of simulation data. PINNS are capable of handling intricate shapes, varying material properties, and integrating experimental data. The data integration capability of PINNS make them even more reliable for quite accurate predictions.

Physics informed Neural Networks (PINNS)

Physics-Informed Neural Networks (PINNs) are a category of machine learning models that integrate physical principles, such as differential equations and boundary conditions, into neural network frameworks. The goal of PINNs is to merge the capabilities of deep learning with the underlying equations of a physical system, thereby enabling precise predictions and the exploration of previously unknown physical phenomena. The primary components of PINNs include:

- Neural Network Architecture: This is composed of layers of neurons interconnected to process and modify input data. The architecture can vary depending on the specific problem and the intricacy of the physical system being simulated.

- Physics-Informed Loss Function: This coalesces different types of losses in order to satisfy the physics of the problem subjected to certain boundary constraints

- Differential Equation Representation: Differential equation is the basis for the physics behind the phenomena. It captures the relation between the solution and input variable through certain derivate components. PINN is formulated to approximate the solution by considering this Differential equation as the physics of the problem

- Boundary and Initial Conditions: These boundary conditions act as the additional constraints to be satisfied along the Differential equation during training. The boundary conditions may be of Dirichlet, Neumann, Robin type. PINN should be able to incorporate these BC and IC's during training and ensure the predictions are aligned with prescribed Boundary and Initial conditions.

- Collocation Points Utilization: These are the points located within the domain which are used to train the PINN to satisfy the governing equation.

Physics informed neural networks uses Automatic differentiation technique using Pytorch or TensorFlow for developing the components to form the governing equation.

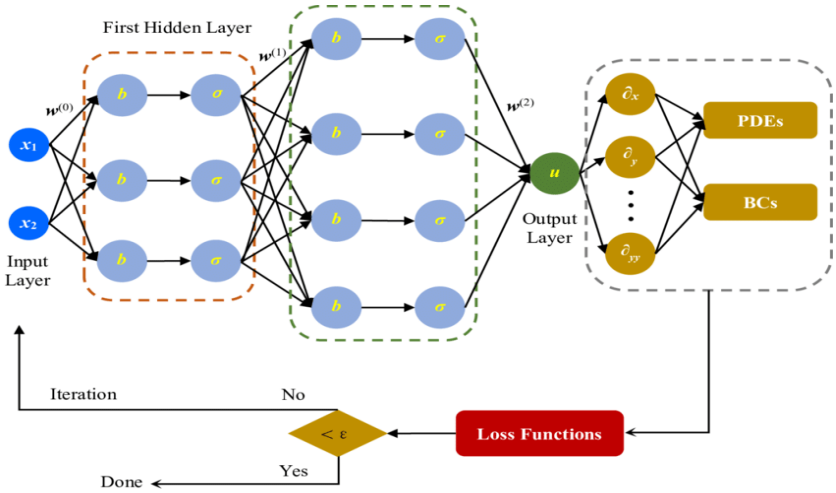

Fig 1.3. Workflow of PINN [3]

Working of PINN

DOMIAN

- We consider PDEs in numerical simulations within a bounded domain.

$$\text{Let } \tilde{\Omega} = \Omega \times [0, T] \text{ where } \Omega \subset \mathbb{R}^d \text{ and } d \in \mathbb{N}$$

BOUNDARY AND INITIAL CONDITIONS

- The boundary is defined as $\partial\Omega = \partial\tilde{\Omega} \times (0, T) \cup \Omega \times \{0\}$
- This implies that numerically, the boundary and initial data are treated equally.

FORMATION OF PDE

- For a point $x = (x_1, \dots, x_d, t)^T \in \tilde{\Omega}$, we consider a PDE.
- The PDE with solution $u: \tilde{\Omega} \to \mathbb{R}$ is denoted as:

$$f(x, D^{k_1}u, \dots, D^{k_m}u) = 0, \text{ for } x \in \tilde{\Omega}.$$

$$\mathcal{B}(u, \boldsymbol{x}) = 0, \ \boldsymbol{x} \in \partial\tilde{\Omega}.$$

Training Process of PINN

1. Construct Neural network which acts as surrogate solution for u
   Let $u^{\Theta}: \mathbb{R}^d \to \mathbb{R}$ be a Feedforward Neural Network (FNN):
2. Define your Domain and PDE:
   Let $u: \tilde{\Omega} \to \mathbb{R}$ be the solution of the PDE given by $f(x, D^{k_1}u, \dots, D^{k_m}u) = 0$

   Where

$$D^{\boldsymbol{k}}u = \partial_{x_1}^{k_1} \cdots \partial_{x_d}^{k_d}$$

3. Boundary and Initial Conditions:

   The boundary and initial conditions are defined as $B(u, x) = 0$ for $x \in \tilde{\Omega}$.

4. PINN Loss functions:
   For given sets of training points $T_f \subset \tilde{\Omega}$ and $T_b \subset \partial\tilde{\Omega}$, the PINN loss $L_T : \mathbb{R}^{\mu} \to \mathbb{R}$ is defined as

$$\mathcal{L}_{\mathcal{T}}(\Theta) = w_f \mathcal{L}_{\mathcal{T}_f}(\Theta) + w_b \mathcal{L}_{\mathcal{T}_b}(\Theta)$$

Where,

$$\mathcal{L}_{\mathcal{T}_f}(\Theta) = \frac{1}{|\mathcal{T}_f|}\sum_{\boldsymbol{x}\in\mathcal{T}_f} \left\|f\left(\boldsymbol{x}, D^{\boldsymbol{k}_1}\hat{u}, \ldots, D^{\boldsymbol{k}_m}\hat{u}\right)\right\|_2^2,$$

$$\mathcal{L}_{\mathcal{T}_b}(\Theta) = \frac{1}{|\mathcal{T}_b|}\sum_{\boldsymbol{x}\in\mathcal{T}_b} \| \mathcal{B}(\hat{u}, \boldsymbol{x}) \|_2^2$$

w_f, w_b are the weights that enforces PINN to perform optimization by taking these as importance of PDE residual and Boundary residual respectively.

Chapter 2

Literature Review

2.1 Thermal Modelling of WAAM

Understanding of Heat transport, solidification behavior, associated residual stresses and distortion requires robust thermal modelling of metal additive manufacturing as which forms a base to conduct these studies.

Ding et al [4] proposed that a heat source model with uniform distribution offers significant benefits regarding processing time due to its insensitivity to mesh configuration. Validating the model's simulated temperature profiles and distribution against experimental measurements from thermocouples and a high-temperature thermal imaging camera instills confidence.

Edison et al. [5] explored how multi-layered deposition affects the estimation and confirmation of melt pool shapes and thermal processes. Their study used finite element analysis to take into account the heat dissipation due to convection and radiation on the additive manufacturing layer surfaces. They employed the element birth and death method to simulate the additive layering of continuous wire. On the base material, various elements were added to form rectangular builds. They conducted a 3D transient nonlinear heat transfer analysis to predict the temperature variations during the entire welding and cooling phases of the procedure, which included the base substrate and two to three layers of cast IN-738LC alloy. Figure 2.1 illustrates the predicted thermal contours and the temperature cycles at certain nodes.

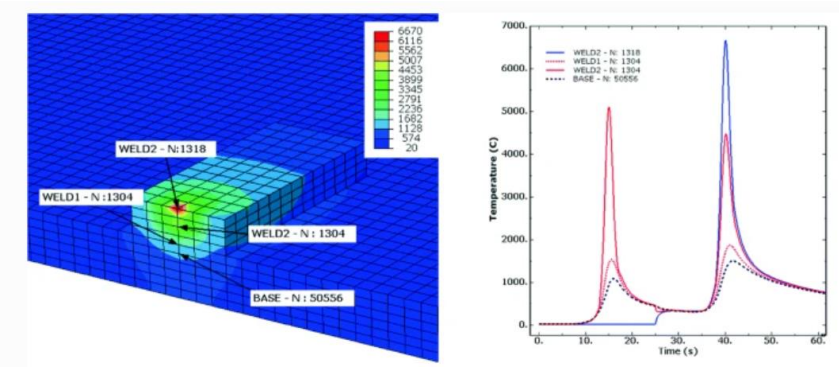

Fig 2.1. Thermal modelling in FEM and thermal cycle of multi-layer built [5]

Ding J et al. [6], reported that the double ellipsoid heat source model proposed by Goldak et al., is commonly used in the FEM analysis of WAAM as shown in figure 2.2

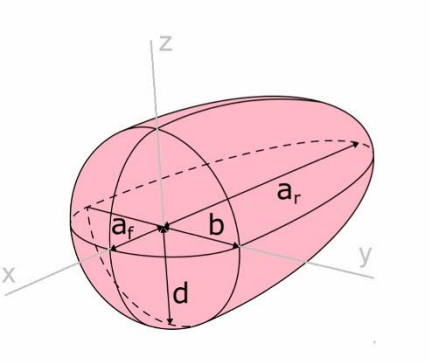

Asymmetric Gaussian Distribution

$$\dot{q} = \frac{6\sqrt{3}\dot{Q}f_{f,r}}{\pi\sqrt{\pi}a_{f,r}bd}\exp\left\{-3\left(\frac{x^2}{a_{f,r}^2}+\frac{y^2}{b^2}+\frac{z^2}{d^2}\right)\right\}$$

Fig 2.2 Goldak double ellipsoidal heat source [6]

Where,

b = half width mm d = Depth of weld pool mm af, ar = Semi axis length mm (front and rear)

Graf et al.[7], and Ahmad et al.[8], identified that in some cases, the calculated temperatures can go above the evaporation temperature by using above heat source model and require modification of the intensity parameter in equation.

To solve this issue, Montevecchi et al [9]. proposed a three-fold solution

- Dividing heat input Q equally between base Q_b and filler Q_w.

- Applying double ellipsoid power density $\dot{q}_b$ for the base, substituting $\dot{Q}$ with $\dot{Q}_b$.
- Use a constant power density distribution $\dot{q}_w = \frac{\dot{Q}_w}{V_{el}}$ for the filler

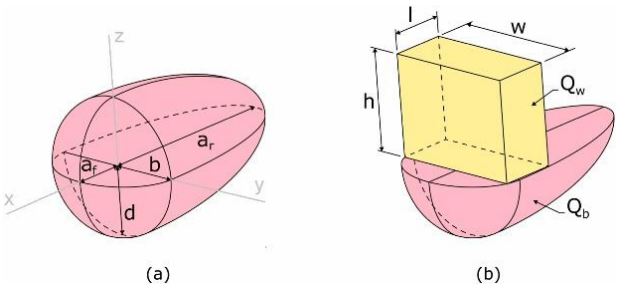

Fig. 2.3 (a) The double ellipsoid heat source model and (b) Proposed Droplet Volume approach in WAAM [9].

Droplet volume V_{el} = l*w*h is represented as a box where heat $\dot{q}v$ is applied to simulate deposition and melting.

Mohebbi et al.,[10] suggests that the differences in the melt pool cross sections of arc welding and WAAM should inevitably give rise to differences in the melting efficiency of both processes due to differences in the heat transferred to the solid metal and lost to the environment. In particular, the approximate semi-infinite plate heat transfer conditions of arc welding are different from the approximate one-dimensional heat transfer conditions of material deposition in WAAM.

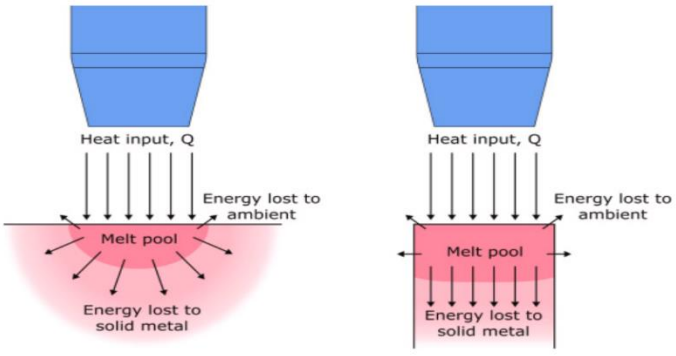

Fig. 2.4 Difference of melt pool cross sections between arc welding and WAAM [10]

Huihui et al.,[11] have investigated the thermal behaviour of a ten-layer single-pass deposition. A 3D transient heat transfer simulation that accounts for temperature-dependent material properties has been conducted to assess the development of the temperature field, the characteristics of thermal cycling, temperature gradients, and the influence of deposition directions on the thermal dynamics of single-pass, ten-layer rapid prototyping. The simulation results align closely with experimental data. The research suggests that the condition for heat dispersion in the melt pool worsens with increasing deposition height. However, maintaining other conditions constant, optimizing the direction of deposition can significantly improve heat dispersion. It is found that consistent deposition directions result in better heat diffusion compared to alternating directions. Although rapid prototyping using welding shares the same heat source as conventional welding, notable differences in thermal processes exist, which include:

- Variations in the ratio of volume,
- Distinct thermal cycles,
- Unique key issues specific to the process,
- Varied paths of deposition.

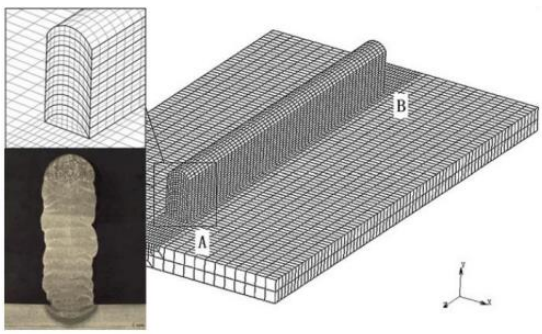

Figure 2.5 3D Finite element model [11].

Figure 2.5 as presenting a 3D finite element model with a focus on points A and B. In Figure 2.6, there are two types of lines: the actual line, representing data measured by a thermocouple, and a dashed line, depicting the modeled thermal cycle curve. This information is illustrated below.

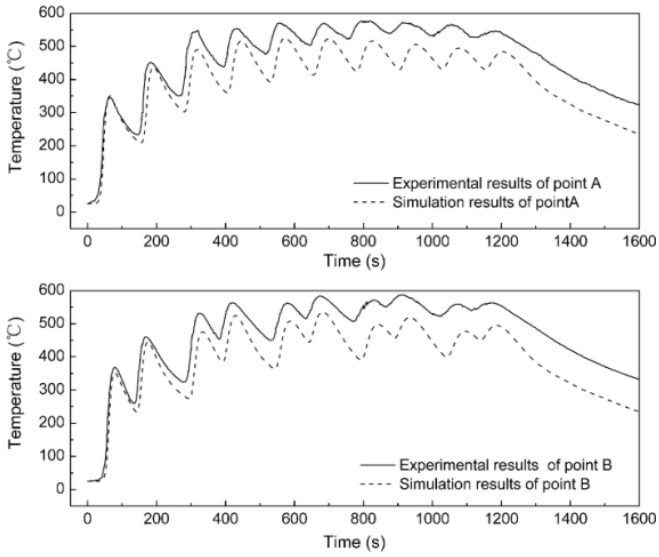

Figure 2.6 Comparison of Simulation & Experimental results [11]

They also examine how the pattern of fabrication influences the temperature gradient. It notes that as the height of deposition increases, leading to higher heat loss, the temperature gradient within the molten pool decreases. In the context of weld-based rapid prototyping, it is observed that the temperature gradient is more pronounced when depositing in the same direction compared to the reverse direction. This observation is illustrated in Figure 2.7

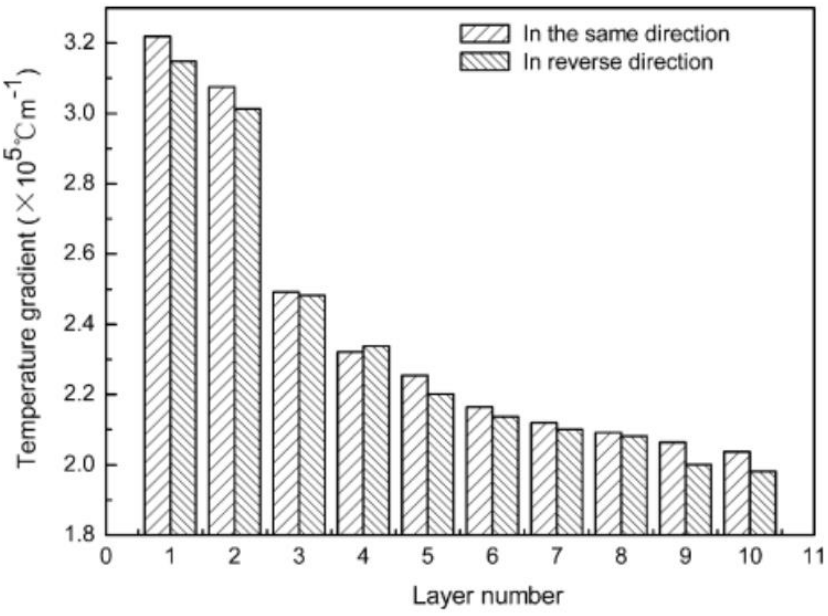

Figure 2.7 Comparison of Temperature Gradients [11]

2.2 Contributions in PIML and Applied PINNS

Lagaris et al.,[9] proposed ANN's for solving differential equations

$$G(\vec{x}, \Psi(\vec{x}), \nabla\Psi(\vec{x}), \nabla^2\Psi(\vec{x})) = 0,\ \vec{x} \in D$$

Subjected to certain boundary conditions (BC's), for instance Dirichlet and/or Neumann conditions, Domain D and its boundary S into a set of points $\hat{D}$ and $\hat{S}$, respectively.

The problem is then transformed into the following system of equations:

$$G\left(\vec{x}_i, \Psi(\vec{x}_i), \nabla\Psi(\vec{x}_i), \nabla^2\Psi(\vec{x}_i)\right) = 0, \forall \vec{x}_i \in \hat{D}$$

If $\Psi_t(\vec{x}, \vec{p})$ denotes a trial solution with adjustable parameters $\vec{p}$, the problem is transformed to:

$$\min_{\vec{p}} \sum_{\vec{x}_i \in D} \left(G\left(\vec{x}_i, \Psi_t(\vec{x}_i, \vec{p}), \nabla\Psi_t(\vec{x}_i, \vec{p}), \nabla^2\Psi_t(\vec{x}_i, \vec{p})\right)\right)^2$$

Proposed Method:

$$\Psi_t(\vec{x}) = A(\vec{x}) + F(\vec{x}, N(\vec{x}, \vec{p}))$$

- $A(\vec{x})$ contains no adjustable parameters and satisfies the BC's.
- where $N(\vec{x}, \vec{p})$ is a single-output feedforward neural network with parameters $\vec{p}$ and n input units fed with the input vector $\vec{x}$.

Brett Bowman et al. [12] applied PINNs to a 1-D Advection–Diffusion–Reaction equation modeling laser energy interaction with skin tissue.

Fig 2.8: From left to right: epidermis, dermis, and fat [12]

They suggested that random sampling is best choice than Latin Hypercube sampling in case of presence of heat source term and strictly suggested that Hybrid activation and Tanh activation functions might be most effective for PDEs with source terms in PINN models.

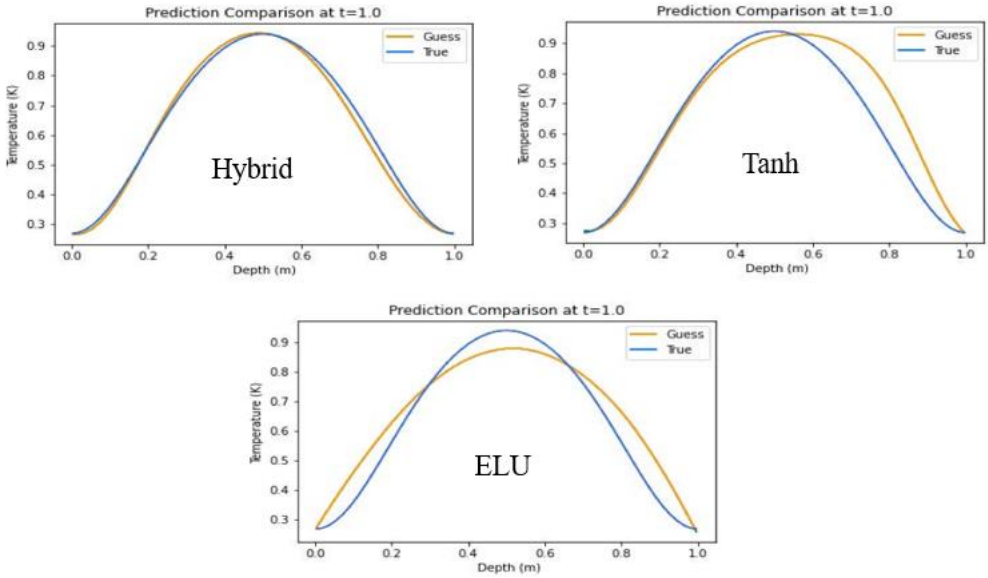

Fig 2.9: Predicted Temperature using different activation functions [12]

Navid et al [13], developed a method to address the conductive heat transfer partial differential equation (PDE), integrating it with convective heat transfer PDEs as boundary conditions. As illustrated in Figure after 50,000 training iterations, the model's predictions for the central part of the object are compared with those derived from Finite Element (FE) analysis. All network models consistently and accurately predict temperature patterns within the trained area. However, shortly after exiting this trained area, all model solutions start to deviate from the FE analysis. To accurately represent the physics beyond the trained zone, only the Physics-Informed Neural Network (PINN) with physics-informed activation functions proves effective. This effectiveness is attributed to PINN's use of physics-informed functions, which more precisely replicate the dynamics of heat transfer in the problem.

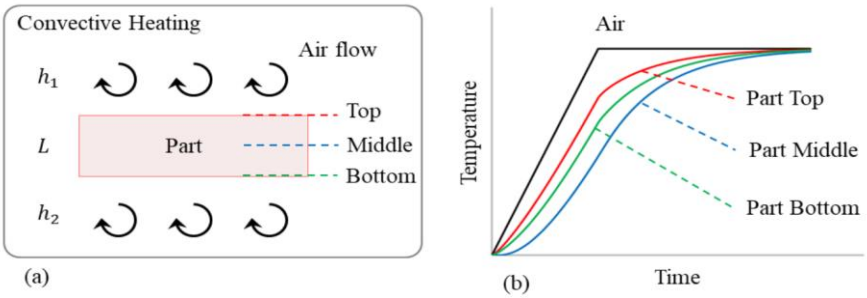

Fig 2.9(a): Convective heating of a part [13]

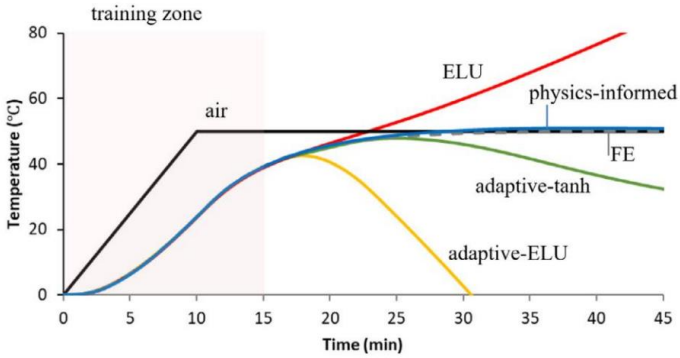

Fig 2.9(b): Convective heating of a part [13]

The accuracy of the trained Physics-Informed Neural Network (PINN) was verified in various one-dimensional and two-dimensional heat transfer scenarios by comparing its predictions to Finite Element (FE) analysis data. The performance and precision of PINN were also evaluated against a traditional Neural Network (NN) that lacked feature engineering. The results showed that both NN and PINN align with FE data within the training domain, but only PINN equipped with engineering features can accurately forecast results outside this domain by effectively capturing the underlying physical principles of the problem.

Jorrit Voigt et al [14] developed a model for dynamic 3D heat transfer in laser material processing, utilizing Physics-Informed Neural Networks (PINNs). This model focuses on dynamic heat conduction in bulk materials, governed by the time-dependent heat conduction equation, a partial differential equation in space ($\vec{x}$) and time (t) :

$$c_p \frac{\partial}{\partial t} u(\vec{x}, t) = \frac{\kappa}{\rho} \Delta u(\vec{x}, t) + \dot{Q}(\vec{x}, t)$$

The temperature field is modelled within a finite cube. To its lower base a Dirichlet boundary condition (BC) was applied and set to 0.

For the four lateral faces (F) the Neumann BC was

$$\frac{\partial}{\partial t} u(\vec{x}, t) = 0.1$$

The initial conditions (IC) were set to $u = 0$ for the whole domain. These conditions are motivated by the typical setup in the laser powder bed fusion process (PBF-LB/M).

For the heat source a Gaussian beam profile with a laser power $P_L = 1$ W and a velocity of 1 mm/s was used. The heat source is modelled by:

$$\dot{Q} = \frac{2 \cdot P_L}{\pi \cdot r_{\text{spot}}^3} \cdot \exp\left(-2 \cdot \frac{r_{\text{focus}}^2}{r_{\text{spot}}^2}\right).$$

The size of the laser spot (r_{spot}) was 0.1 mm and the position of the laser focus (r_{focus}) was a function of time.

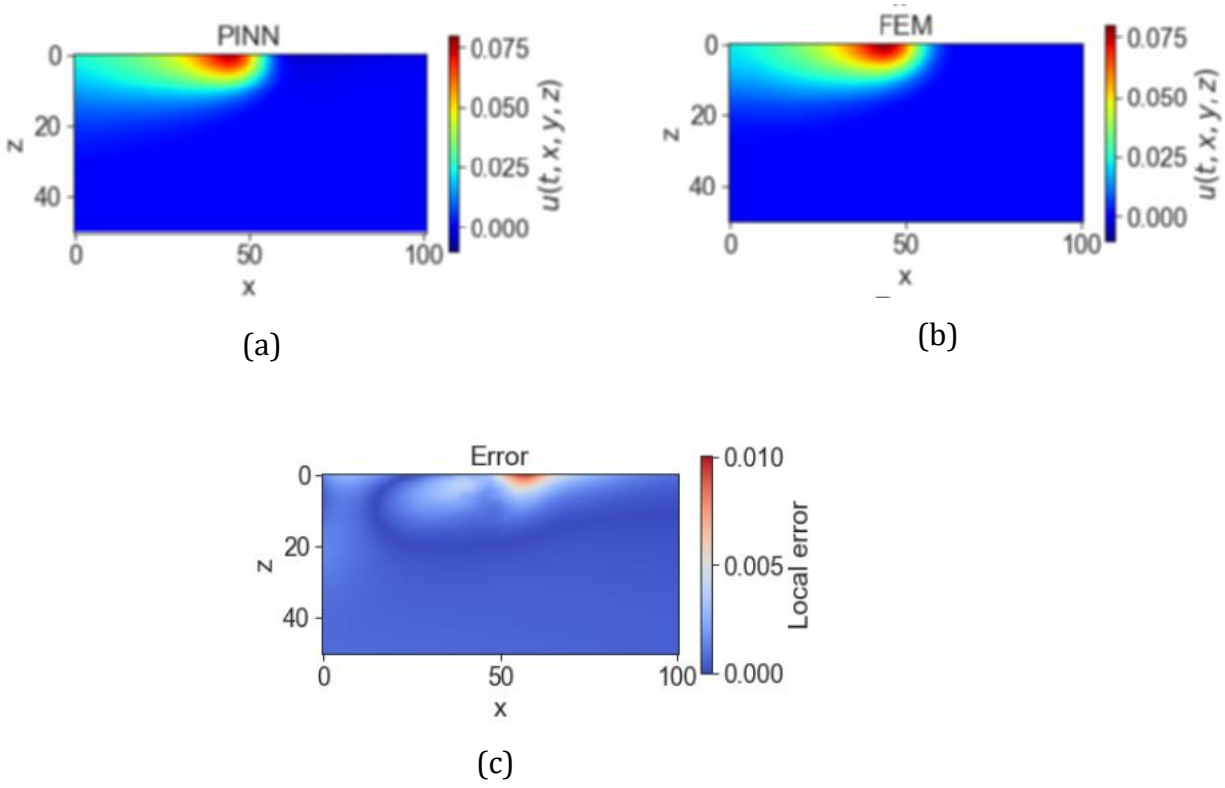

Fig 2.10: (a) Predicted temperature by PINN (b) FEM solution (c) Absolute Error [14]

To reduce the computational load, the approach does not calculate errors from the governing equation at every point in the lattice. Instead, it stochastically samples these errors from a sufficiently dense subset of lattice points, targeting about 20% in each epoch. For the computations, a total of 40,000 collocation points were utilized, selected through the Latin-Hypercube sampling method. This technique helps in efficiently approximating the error distribution while managing the numerical effort required.

Qiming Zhu et al [15] proposed an idea of considering the Dirichlet BC in Hard approach rather than conventional Soft approach.

A particular portion of the neural network to purely satisfy the prescribed Dirichlet BC.

For that, we first define a Heaviside function as

$$H_\epsilon(\boldsymbol{x}) = \begin{cases} 1 - \cos\left[d(\boldsymbol{x})\pi/\epsilon\right] & \text{if } d(\boldsymbol{x}) < \epsilon \\ 1 & \text{if } d(\boldsymbol{x}) \geq \epsilon \end{cases}$$

$$\boldsymbol{u}_{NN} = \boldsymbol{u}_{bc}[1 - H_\epsilon(\boldsymbol{x})] + \boldsymbol{u}H_\epsilon(\boldsymbol{x})$$

$$p_{NN} = p_{bc}[1 - H_\epsilon(\boldsymbol{x})] + pH_\epsilon(\boldsymbol{x})$$

$$T_{NN} = T_{bc}[1 - H_\epsilon(\boldsymbol{x})] + TH_\epsilon(\boldsymbol{x})$$

where $d(\boldsymbol{x}) =$ distance to the Dirichlet boundary, $\epsilon =$ artificial thickness of the boundary.

Since $H_\epsilon(\boldsymbol{x})$ smoothly changes from 1 to 0 as $d(\boldsymbol{x})$ approaches to 0, the prediction will automatically satisfy the prescribed values by definition, without needing additional constraint.

Liao et al [16] employed physics-informed neural networks (PINNs) to develop a combined physics-based and data-driven thermal modeling method for additive manufacturing (AM) operations. This approach aims to predict comprehensive temperature histories and identify unknown material and process parameters by integrating partially observed temperature data from an infrared camera with physical laws.

The hybrid thermal modeling framework for AM, based on PINNs, is illustrated in Figure 2.11

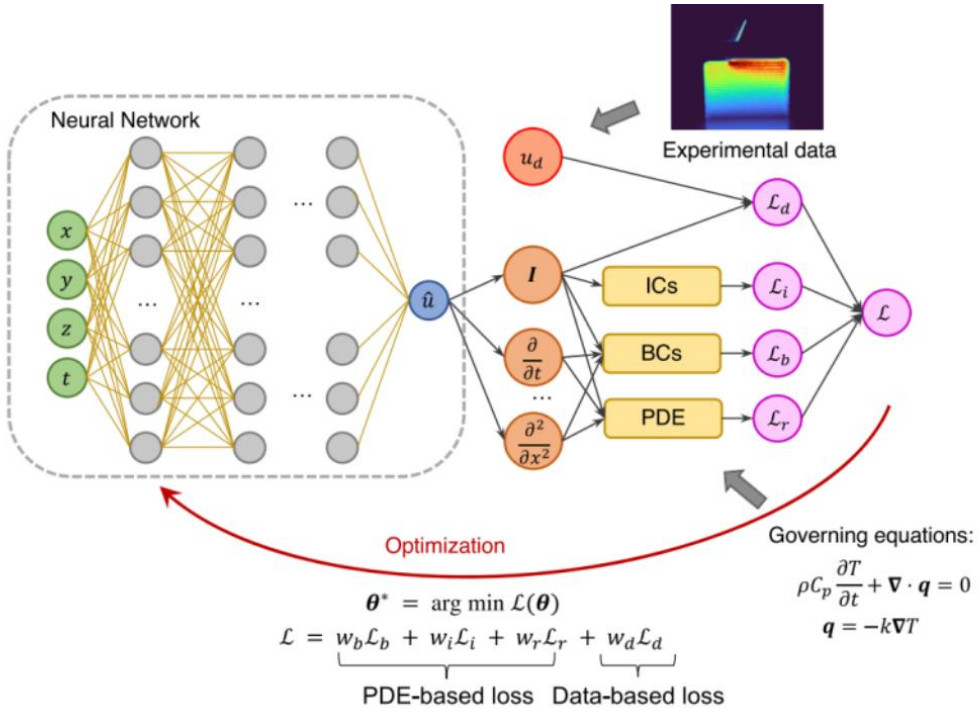

Fig 2.11: Hybrid PINN Workflow [16]

In this workflow, the neural network uses spatial-temporal coordinates to predict temperature at specific locations. The training of the neural network involves a loss function that combines residuals from the partial differential equations (PDEs), boundary conditions (BCs), initial conditions (ICs), and an additional data-based loss term incorporating experimental temperature data.

compares the full-field temperature predictions of the trained PINN model with measured infrared (IR) data. The comparison reveals a Root Mean Square Error (RMSE) of 47.28 K between the predicted temperature field and the data measured at t = 07 seconds, demonstrating the model's accuracy in estimating total field temperature. This example highlights the effectiveness of the hybrid physics-based data-driven framework in seamlessly integrating experimental data into the physics-informed model, providing valuable insights into thermal behavior in AM processes.

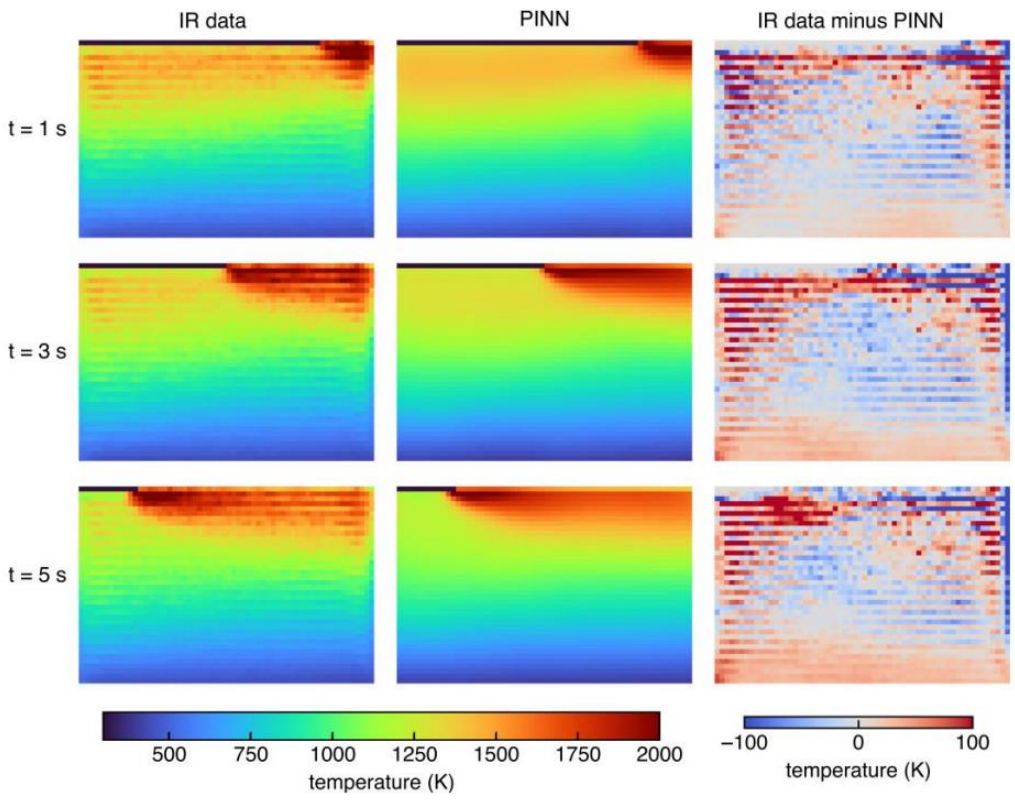

Fig 2.12: Comparison analysis of predicted data and measured IR data [16]

Chapter 3

ML FOR AM: PINN APPROACH

3.1 Governing Equations

Think about a welding torch moving along the x-axis on a flat plate at a constant velocity v. The principle of energy balance (specifically enthalpy) is applied to a designated control volume. This principle dictates that the rate at which enthalpy increases within the control volume should be equal to the total of the rate at which heat flows into the control volume through its surfaces and the rate at which heat is generated within the control volume.

$$\Rightarrow \frac{d}{dt}\int_v H dv = -\int_s \vec{J}\cdot\overrightarrow{ds} + \int_v q dv$$

Using the Fourier's law of heat conduction;

$$\vec{J} = -k\frac{\partial T}{\partial x}$$

Using the divergence to convert surface integral into volume integral in above equation;

$$\Rightarrow \frac{d}{dt}\int_v H dv = -\int_s (\vec{\nabla}\cdot\vec{J}) dv + \int_v q dv$$
$$\Rightarrow \frac{dH}{dt} = \vec{\nabla}\cdot(k\vec{\nabla}T) + q$$
$$\Rightarrow \rho C_p\frac{dT}{dt} = \vec{\nabla}\cdot(k\vec{\nabla}T) + q$$
$$\Rightarrow \frac{dT}{dt} = \frac{k}{\rho C_p}\nabla^2 T + \frac{q}{\rho C_p}$$
$$\Rightarrow \frac{\rho C_p}{k}\frac{dT}{dt} = \nabla^2 T + q$$

where H is enthalpy per unit volume, T is temperature, q is rate of heat generation, $\vec{J}$ is heat flux, $\boldsymbol{\rho}$ is density of material, $\boldsymbol{C_p}$ is Specific heat at constant pressure and $\boldsymbol{\alpha}$ is reciprocal of thermal diffusivity.

Since, we are Considering the heat source is applied as a surface flux, the $q = 0$, since no internal heat generation is present in our study.

Assumptions considered for the Study:

- The latent heat of phase change was neglected in the material properties because it had little impact on the temperature distribution (Single phase study only)
- The internal flow of the melt pool during deposition and heat loss from evaporation were also ignored.
- Thermal properties are kept as constant.
- Initial temperature is considered as room temperature.
- Bottom surface of the plate is kept as insulated surface.

In heat equation, temperature T is function of spatial coordinates ($\boldsymbol{x}$, $\boldsymbol{y}$, $\boldsymbol{z}$) and time t.

3.2 Boundary conditions

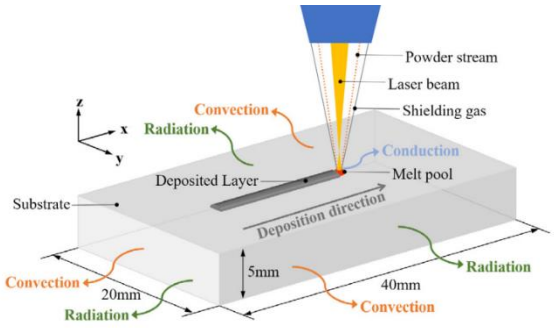

Fig: 3.1 Schematic of Process physics with Boundary condition of Metal Additive process [18]

The Heat source flux is assumed to be applied on only the top surface while the convective and radiative heat flux are applied on all surfaces and can be expressed as

$$-k\vec{\nabla}T.n = qheat\ source + q\ rad + q\ conv$$
$$q_c = h_c(T - T_a)$$
$$q_r = \sigma\epsilon\left(T^4 - T_a^4\right)$$

$\boldsymbol{n}$ = [n_x, n_y, n_z], Unit normal vector on the surface

For the bottom surface of the substrate, where a Dirichlet boundary condition is applied:

$$T_{|z=0} = T_0$$

3.3 IMPLEMENTATION OF PINN MODEL:

3.3.1 3D temperature field without labeled data in process of laser DED

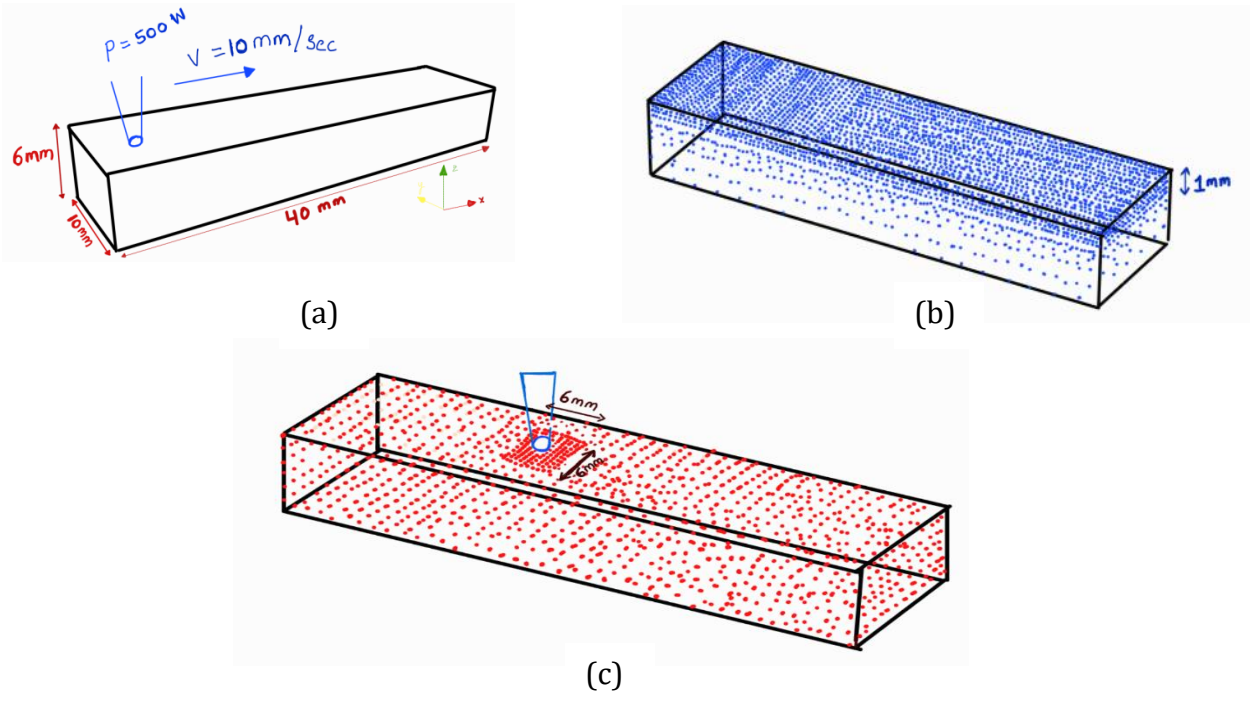

Fig 3.2: (a) Domain considered for the study (b) Finer point distribution on top layer upto 1mm depth , (c) Square mesh considered around the moving heat source for capturing Surface Heat flux

Point discretisation strategy of domain followed:

- The domain, measuring 40x10x6 mm, was point wise distributed at 1 mm intervals with a time step of 0.05 seconds
- The top layer (40x10 mm up to 1 mm depth) was point wise distributed at a finer interval of 0.5 mm due to higher thermal gradients.
- Near toolpath origin also, more points were sampled with mesh grid of 4*4 mm with 0.5 mm intervals for ease of capturing the temperature of surrounding particles from initial state, when heat source is just about to start from its origin
- To effectively model the heat source dynamics in Metal AM, a finer mesh grid of 6x6 mm with 0.25 mm intervals was used near the source area.

Process and Material Properties:

Laser Parameters	
Laser Power (P)	500 W
Radius of Laser (r)	1.5 mm
Laser absorptivity (η)	0.4
Laser Speed (V)	10 mm/s

Table 3.1: Laser Parameters

Material Properties	
Specific Heat Capacity (C_p)	0.5 J/kg.
Thermal conductivity(K)	0.01 W/mk
Emissivity (ε)	0.3
Thermal conductivity(K)	0.01 W/mk
Maximum Temperature range	3000 K

Table 3.2: Material Properties for L-DED

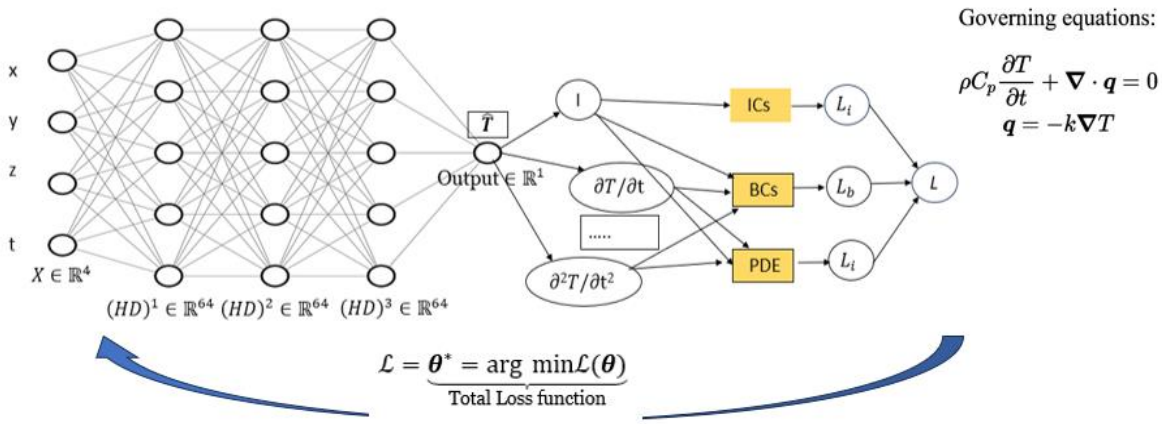

Fig 3.3 : PINN Architecture Followed

A 3-dimensional transient heat transfer analysis subjected to boundary and initial conditions as discussed above has been implemented in the PINN model using custom sampling strategy as discussed earlier.

The input layers takes the space and time coordinates, The architecture consists of 3 hidden layers each $\epsilon\mathbb{R}^{64}$ and the output layer $\epsilon\mathbb{R}^{1}$ predicts the temperature variable. Automatic differentiation technique is used to form the required components of PDE and a combined loss function is constructed which is a weighted sum of all the different losses (BC Loss, IC Loss, PDE Loss) as shown below.

Network and training parameters:

Parameter	Value
Layer Architecture	[4, 64, 64, 64, 1]
Activation function	Linear, Tanh for Hidden layers, Softplus for output
Epochs	80000
Learning rate	2e-4
Input Transform	Normalization between [-1, 1]

Table 3.3: PINN Network Parameters for L-DED

Loss Functions:

$$Boundary\ Loss: \quad \mathcal{L}_b = \frac{1}{N_b}\sum_{k=1}^{N_b} \left|\mathcal{B}\left(\hat{T}\left(\boldsymbol{x}_b^k, t_b^k\right), \boldsymbol{x}_b^k, t_b^k\right)\right|^2,$$

$$Initial\ Loss: \quad \mathcal{L}_i = \frac{1}{N_i}\sum_{k=1}^{N_i} \left|\hat{T}\left(\boldsymbol{x}_i^k, 0\right) - I\left(\boldsymbol{x}_i^k\right)\right|^2,$$

$$PDE\ Loss: \quad \mathcal{L}_r = \frac{1}{N_r}\sum_{k=1}^{N_r} \left|\hat{T}\left(x_r^k, t_r^k\right) - \mathcal{N}[\hat{T}]\right|^2,$$

where N_b, N_i, and N_r are the number of the sampling points for each loss term

Combined Loss:

$$L = w_b L_b + w_i L_i + w_r L_r$$

Where w_b, w_i, w_r are the weights considered as each loss in order to adjust the importance on the which loss to be optimized as per the training situation

Results and Discussion

After hyper parameter tuning and architectural changes, it has been found that a learning rate of 2e-4 and architecture of [4, 64, 64, 64, 1] with 80000 epochs found be to converged and results are as follows:

Loss function minimization

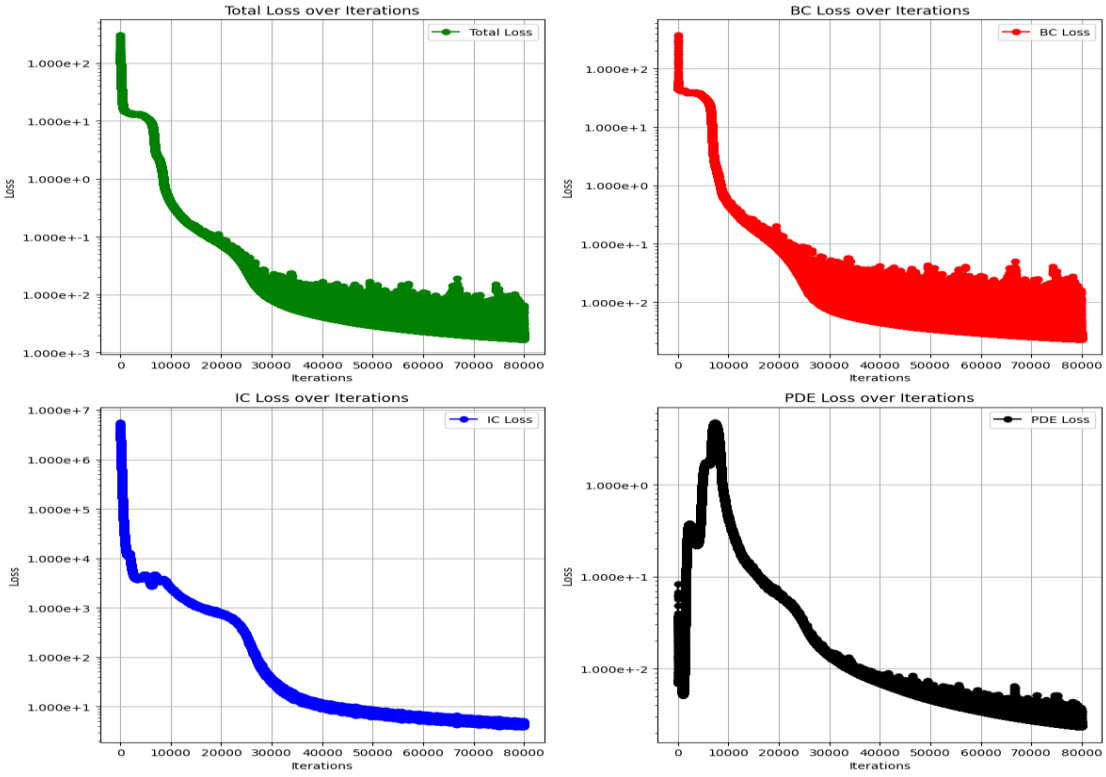

Fig 3.4: Loss Curves

Loss	Value
Total Loss	3.221e-03
BC Loss	1.128e-02
IC Loss	4.784e+00
PDE Loss	2.759e-03

Traning time	Nearly 5.2 hrs on P100 16GB GPU

Model Predictions:

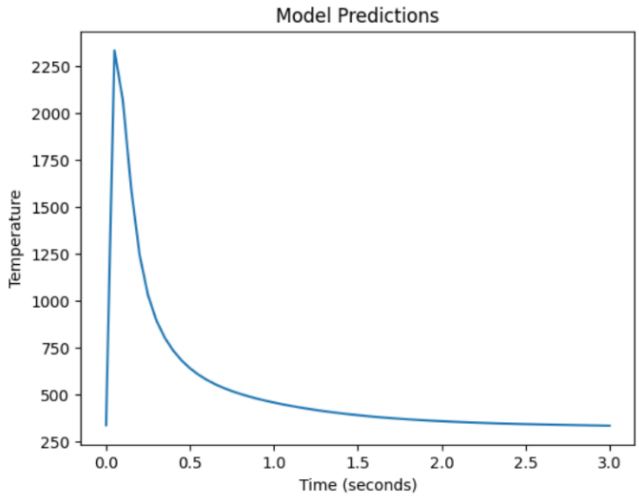

Fig 3.5 (a) Temperature curve predicted
At x, y, z = (5.0, 5.0, 6.0) (Top Surface)
6 Time steps (step size= 0.5 sec) up to 3 sec

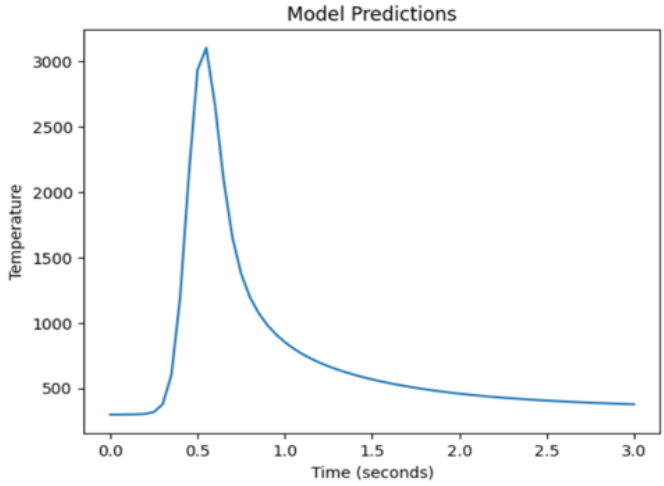

Fig 3.5 (b) Temperature curve predicted
At x, y, z = (10.0, 5.0, 5.0, 6.0) (Top surface at Arbitrary location with 6 Time steps
(step size= 0.5 sec) up to 3 sec

Predicted Thermal cycles and Temperature distribution:

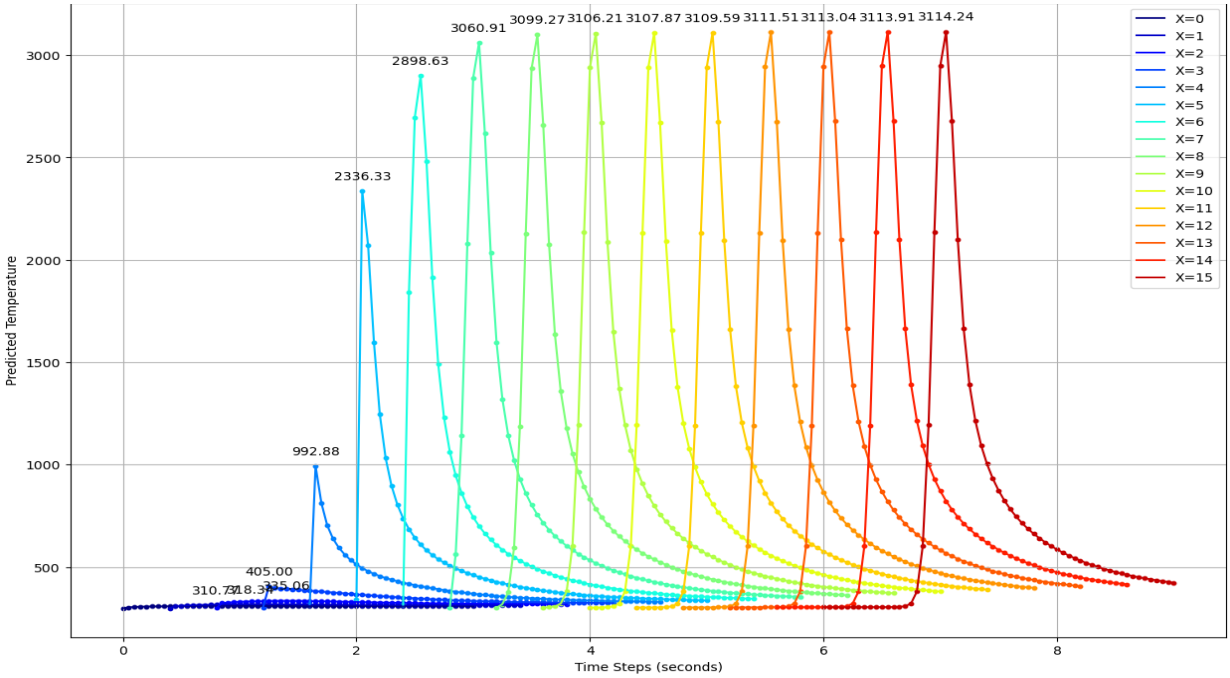

Fig 3.6 (a) Predicted Thermal cycles along 15 mm length from start (X= 0)

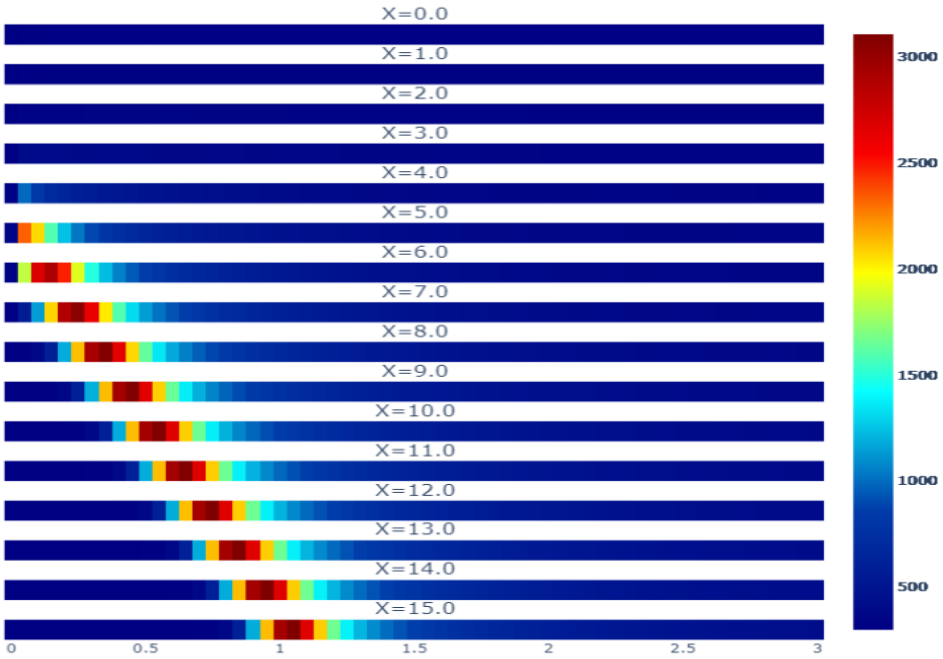

Fig 3.6 (b) Temperature distribution along the track

3.3.2 3D Transient Thermal analysis on Wire arc Additive Manufacturing

Wire arc additive manufacturing (WAAM) developed from gas metal arc welding (GMAW), gas tungsten arc welding (GTAM), or plasma arc welding (PAW) is regarded as the most suitable candidate to fabricate large scale metallic structure for the high deposition rates and low feedstock and equipment costs.

In this section we will carry out a 3D transient thermal analysis on GMAW based Wire arc additive Manufacturing using PINN model.

The Boundary and Initial conditions for the process remains same as that of laser DED seen earlier. The major change comes with the heat source, where in WAAM we majorly use Goldak double ellipsoidal heat source as shown below.

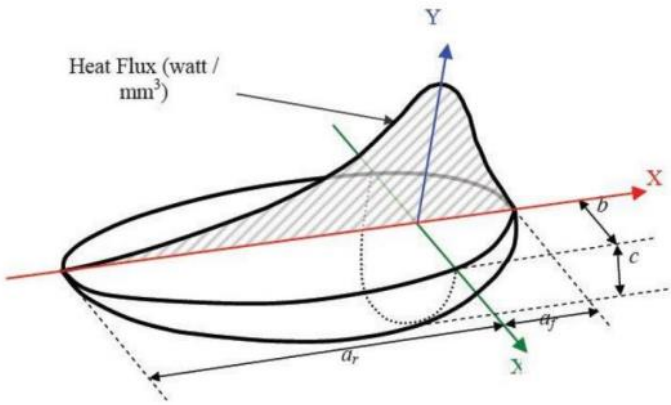

Fig 3.7: Goldak Double Ellipsoidal Heat Source [19]

$$q_{\text{arc}} = \begin{cases} \dfrac{6\sqrt{3} f_{\text{f}} \eta U I}{a_{\text{f}} b c \pi \sqrt{\pi}} \exp\left(-3\left(\dfrac{(x-x_0-V_{\text{T}}t)^2}{a_{\text{f}}^2} + \dfrac{(y-y_0)^2}{b^2} + \dfrac{(z-z_0)^2}{c^2}\right)\right) & ((x-x_0-V_{\text{T}}t) > 0) \\ \dfrac{6\sqrt{3} f_{\text{r}} \eta U I}{a_{\text{r}} b c \pi \sqrt{\pi}} \exp\left(-3\left(\dfrac{(x-x_0-V_{\text{T}}t)^2}{a_{\text{r}}^2} + \dfrac{(y-y_0)^2}{b^2} + \dfrac{(z-z_0)^2}{c^2}\right)\right) & ((x-x_0-V_{\text{T}}t) < 0) \end{cases}$$

Parameter	Value (mm)
Front semi-axis length (a_f)	1.002
Rear semi-axis length (a_r)	3.34
Half width of arc (b)	1.67
Depth of arc (c)	1.67
Gaussian distribution	3

The major change when performing this analysis comes with the Custom point wise distribution near the heat source which plays a very significant role as the distribution of heat is asymmetric Gaussian distribution.

- The Governing equations and boundary conditions discussed previously are pretty much valid here as well, The major change comes with the asymmetric gaussian heat flux distribution.
- Due to this, instead of square bounded finer mesh grid near heat source, a rectangular mesh grid of approximately 9*12 mm is considered.
- And remaining part of distribution is exactly same as that of earlier application

Process parameters and material properties:

Process Parameters	
Current (I)	500 W
Voltage (U)	15.3 V
Heat transfer Efficiency (η)	0.9
Travel Speed (V)	10 mm/s

Table 3.4 WAAM setup Parameters

Material Properties	
Material	IN718
Density (p)	8e-3 g/cm^3
Specific Heat Capacity (C_p)	0.5 J/gk
Thermal conductivity(K)	0.05 W/mk
Emissivity (ε)	0.3
Convective Heat transfer Coefficient (h)	2e-5
Maximum Temperature range	1800 K

Table 3.5 Material properties considered for WAAM

Results and Discussion:

Parameter	Value
Layer Architecture	[4, 64, 64, 64, 1]
Activation function	Linear, Tanh for Hidden, Soft-plus for Output Transform
Input Transform	Normalized between [-1, 1]
Optimizer	Adam

Table 3.6 PINN Network Parameters for WAAM

After trying the hyperparameter tuning, the following results are obtained

Sr.no	Learning rate	Weight importance (BC, IC, PDE)	epochs	Loss values	Remarks
1	2e-4	[1, 1e-4, 1]	50000	It: 49900: Loss: 3.219e-01, BC: 4.299e-01, IC: 1.481e+03, PDE: 3.878e-01,	
2	2e-3	[1, 1e-4, 1]	100000	It: 99900: Loss: 1.43e-01, BC: 3.312e-01, IC: 1.481e+02, PDE: 2.344-01,	
3	2e-4	[1, 1e-2, 1]	80000	It: 79900,Loss:3.104e+00, BC: 2.581e+00, IC: 4.941e+02, PDE: 1.788e+00, Time: 29.98 sec	Found as good direction of tuning Getting advantage in time also
4	2e-4	[1.5, 1, 1.5]	60000	It: 59900, Loss: 8.347e+00, BC: 7.924e+00, IC: 3.043e+00, PDE: 4.143e+00, Time: 29.85	*Latest

Table 3.7: Parameter tuning and their respective Loss values

After hyper parameter tuning and architectural changes, it has been found that a learning rate of 2e-4 and architecture of [4, 64, 64, 64, 1] with 60000 epochs found be to converged well and results are as follows:

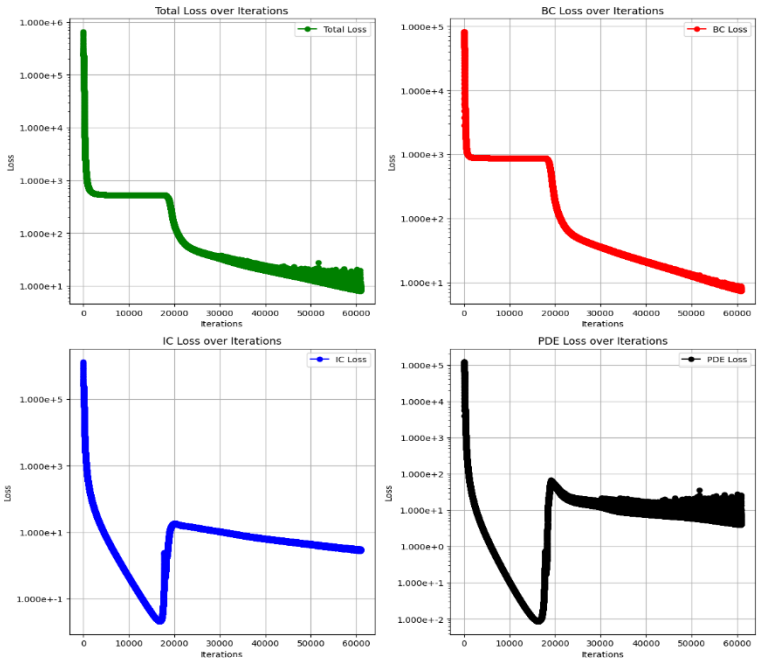

Fig 3.8 Loss curves

Loss	Value
Total Loss	8.347e+00
BC Loss	7.924e+00
IC Loss	3.043e+00
PDE Loss	4.143e+00

Training time	Nearly 5 hrs on P100 16GB GPU

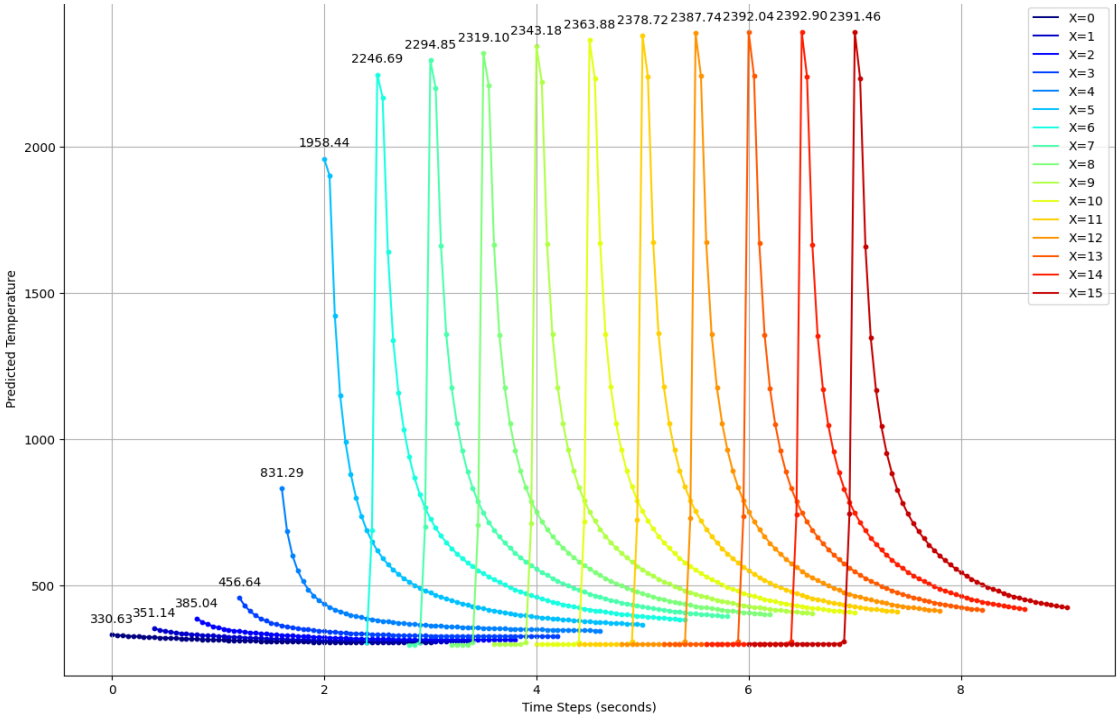

Fig 3.9 Thermal cycle along the track of 15 mm

Challenges:

- Time taken for training of the model is high
- Network architecture is unable to capture the thermal cycle just before the start of heat source origin

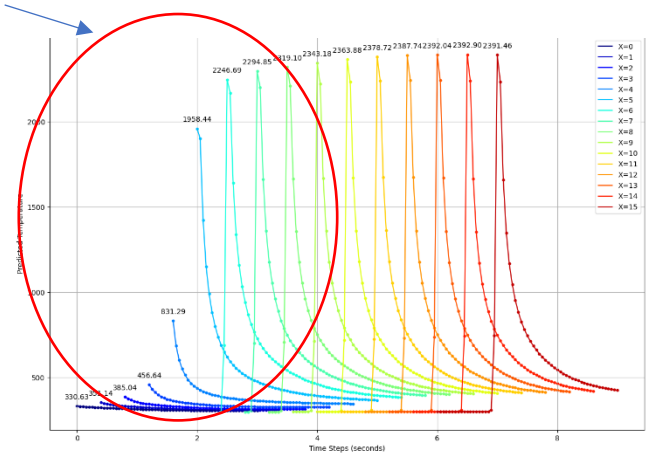

Fig 3.10: Model failed in capturing the initial Thermal cycles near the Heat source origin

Possible Reasons:

- More complex distribution of points near heat source origin may be required
- Temperature dependent material properties
- More optimization of network parameters may be required

Chapter 4

Future Plan of action

- Validation of the Predicted results with help of simulation software
- Incorporate Different Sampling techniques like Latin hypercube Sampling (LHS), More complex distribution of points near heat source
- Integrating heavy function strategy which can reduce the number of points required for the analysis.
- Try to model the same with Hybrid model (data + physics)
- Extend the model for multilayer build.

References

[1] Alagha, Ali & Hussain, Shahadat & Zaki, Wael. (2021). Additive manufacturing of shape memory alloys: A review with emphasis on powder bed systems. Materials & Design. 204. 109654. 10.1016/j.matdes.2021.109654.

[2] Oh, Wook & Son, Jong & Baek, Gyeong & Shim, Do. (2020). Excess deposition for suppressing interfacial defects induced on parts repaired using direct energy deposition. The International Journal of Advanced Manufacturing Technology. 106. 10.1007/s00170-019-04650-w.

[3] Gu, Yan & Zhang, Ch & Zhang, Peijun & Golub, Mikhail. (2022). Enriched physics-informed neural networks for in-plane crack problems: Theory and MATLAB codes.

[4] Ding, Donghong, Shimin Zhang, Qinhua Lu, Zengxi Pan, "The well distributed volumetric heat source model for numerical simulation of wire arc additive manufacturing process," Materials Today Communications, p. 11, 2021.

[5] E. A. Bonifaz, "Modelling of Thermal Transport in Wire + Arc Additive Manufacturing Process," in ICCS, Switzerland, 2019.

[6] Ding, J., et al. "A computationally efficient finite element model of wire and arc additive manufacture." The International Journal of Advanced Manufacturing Technology 70 (2014): 227-236

[7, 8] Graf et al.[7], and Ahmad et al.[8],

[9] Montevecchi, Filippo, et al. "Finite element modelling of wire-arc-additive-manufacturing process." Procedia Cirp 55 (2016): 109-114.

[10] Mohebbi, M.S., Kühl, M. & Ploshikhin, V. A thermo-capillary-gravity model for geometrical analysis of single-bead wire and arc additive manufacturing (WAAM)

[11] H. Zhao, G. zhang, Z. Yin and L. Wu, "A 3D dynamic analysis of thermal behavior during single-pass multi-layer weld-based rapid prototyping," Journal of Materials Processing Technology, p. 8, 2011.

[12] Lagaris, Isaac & Likas, Aristidis & Fotiadis, Dimitrios. (1998). Artificial neural networks for solving ordinary and partial differential equations. IEEE Transactions on Neural Networks. 9. 987-1000. 10.1109/72.712178.

[13] Physics-Informed Neural Networks for the Heat Equation with Source Term under Various Boundary Conditions, Brett Bowman et al.,2023

[14] Navid et al., 2020 A physics-informed machine learning approach for solving heat transfer equation in advanced manufacturing and engineering applications

[15] Voigt, Jorrit & Möckel, Michael. (2022). Modelling dynamic 3D heat transfer in laser material processing based on physics informed neural networks. EPJ Web of Conferences. 266. 10.1051/epjconf/202226602010.

[16] Zhu, Qiming & Liu, Zeliang & Yan, Jinhui. (2021). Machine learning for metal additive manufacturing: predicting temperature and melt pool fluid dynamics using physics-informed neural networks. Computational Mechanics. 67. 10.1007/s00466-020-01952-9.

[17] Shuheng Liao, Tianju Xue, Jihoon Jeong, Samantha Webster, Kornel Ehmann, Jian Cao, "Hybrid thermal modeling of additive manufacturing processes using physics-informed neural networks for temperature 56 prediction and parameter identification.," Computational Mechanics, p. 14, 2022.

[18] Shilin Li, Gang Wang, Yuelan Di, Liping Wang, Haidou Wang, Qingjun Zhou, A physics-informed neural network framework to predict 3D temperature field without labeled data in process of laser metal deposition

[19] Yousef Ghaderi Dehkordi, Anaraki, A.P. & Shahani, A.R. Investigation of Heat Source Models and Process Factors on Temperature and Residual Stress in GTAW of Aluminum Plates. *Russ. J. Non-ferrous Metals* **60**, 450–462 (2019). https://doi.org/10.3103/S1067821219040023